Final Report:
M-Fly Propeller-Wing Interaction

Aero 405 Final Report

M-Fly Propeller-Wing Interaction

University of Michigan – Ann Arbor
Team 2

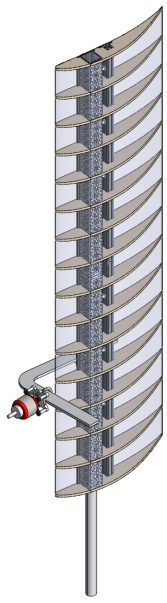

April 23, 2021

Written by:

Isaiah Fleischer, Project Lead
Kalvin Monroe, Engineer
Venkat Subramaniam, Engineer
Elgan Wu, Engineer
Kail Yuan, Engineer

Written for:

Leandro Martinez, Team Captain

Contents

List of Figures

List of Tables

I. Executive Summary

For over a decade, M-Fly Aero Design has designed performance-driven aircraft for the Society of Automotive Engineers (SAE) Aero Design Competition. In our pursuit to maximize our aircraft's performance, we are investigating potential new design ideas. A proposed method to achieve higher performance is to use wing-mounted propellers as opposed to a traditional nose-mounted design. M-Fly has tasked us with characterizing the aerodynamic performance improvements of a wing-mounted propeller, and identifying an optimal propeller location to maximize performance improvements. The purpose of this document is to communicate the results of our study, and provide recommendations on how M-Fly should proceed with this design idea.

Over a 10 week period, the team has designed and constructed a test wing section that models the typical flight conditions of M-Fly aircraft. After thorough testing of the physical test wing in the University of Michigan's 5- by 7-foot wind tunnel, paired with a series of Computational Fluid Dynamics (CFD) validation simulations, we have found the following conclusions:

The test wing had measurable aerodynamic performance improvements due to the introduction of a propulsor and is further dependent on said propulsor's location. We have found that placing the propeller closer to the wingtip, provided that the propeller rotation is opposite to the direction of wingtip effects, significantly decreases drag experienced by the wing. The team recommends that M-Fly place the propellers as far out on the span of each wing as possible such that other design parameters, such as the tip-over angle, and wing structural weight, are still within design constraints.

II. Introduction

The M-Fly Aero Design Team has a successful history in designing, building, and flying RC aircraft. However, nearly all aircraft produced by the team have featured a nose-mounted propeller design. This is primarily because M-Fly has only recently transitioned from combustion engines to electric motors.* With this transition, M-Fly has been able to investigate alternative propeller configurations. The team has found that mounting the propellers on the wings can lead to significant improvements in aircraft mass and aerodynamic performance, but the optimal location for wing-mounted propellers is still unknown. As a result, M-Fly has tasked our team with characterizing the aerodynamic improvements from these wing-mounted designs. Our team has devised a series of experiments to complete this task by quantifying the performance of a scaled M-Fly wing with wing-mounted propellers.

Our team studied the interactions between the propeller and wing and has determined that the maximum spanwise location of the propeller from the wing root best improves wing performance. This was done through constructing a wing section that matched M-Fly flight conditions and building CFD simulations in parallel. The goal of this parallel development is to physically validate any performance increases due to propeller positioning and simultaneously build simulations that can match the results. This provides concrete evidence that this phenomenon can be replicated in software and future M-Fly aerodynamic engineers can utilize the simulations to quantify the

*Internal combustion engines at the RC-scale are historically unreliable and problematic with time constraints at competitions. Adding a second engine would be untenable as it would compound these issues.

trade-offs between propeller positions.

A. Project Applications Towards M-Fly

The findings of this study will be incorporated into future M-Fly designs as its goal is to quantify the effect of propeller placement on the performance of M-Fly aircraft. Specifically, information on the sensitivity of an aircraft's performance with respect to this variable will be of great use in providing justification for the location of each aircraft's propulsion system.

As M-Fly's score in their yearly competition is directly related to their aircraft's performance, this work aims to benefit M-Fly by quantifying the increase in performance of future aircraft designs through wing-mounted propellers. In particular, the current work will be of great benefit for M-Fly's aerodynamics subteam in analyzing the performance of proposed designs prior to physical construction. In addition, M-Fly placing well in their competitions will have the effect of boosting the prestige of the Aerospace Department and University as a whole.

B. Broader Impact

Outside of M-Fly, this project's impact is primarily limited in scope to RC-scale aircraft. There are numerous project teams and research projects being undertaken at the University in this class of aircraft, and our conclusions can be used to help improve the performance of these projects. Furthermore, there are numerous companies creating drones similar in size to M-Fly aircraft, particularly those involved in emergency supply deliveries to remote locations, and we hope that the results of this work can help in refining their designs.

C. Previous Research and Literature Review

Propeller-wing flow interaction, especially in the cruise regime, has been an area of active research for many years. D.H. Wood studied the optimal placement of propellers with respect to vertical and streamwise locations, and found that the ideal placement for a propeller is with the thrust axis in-line with the wing chord-line and 25% of the chord in front of the leading edge. The produces a net propulsive efficiency of approximately 75%. [1] A further report by Wood in 1936 found that adding a propeller to a wing increased its aerodynamic efficiency by approximately 11% at cruise conditions for a passenger aircraft [2].

More recently, a review paper from 2004 by Veldhuis summarized previous research on the topic of propeller-wing interaction. This paper largely agreed with Wood's work, finding that mounting the propeller slightly in front and vertically in-line with the wing was optimal. Further, it showed that the ideal spanwise location is at or near the wingtip [3]. Our project investigated the effects of propeller positioning on wing lift and drag similar to studies discussed in this paper, though on a much smaller and relatively unexplored scale.

In addition to formal literature on the subject, we have found examples of CFD simulations involving rotating propellers in a fluid medium [4], [5]. Performing simulations in the vein of these examples allows us to study propeller-wing interactions prior to constructing a physical model.

Finally, Gilbert et al. [6] found that propellers can increase the maximum lift coefficient of an RC aircraft-sized wing by as much as 29%. This study looked at the vertical propeller mounting distance above and below the leading edge rather than its spanwise location. The results of this study further corroborate the existence of performance increases from propeller-wing interference. This study serves as a precursor to the current study, and we incorporated more rigorous simulations and ensured that our test article accurately represents flight conditions.

D. Experimental Methods and Techniques of Study

We set up our experiment to closely mimic a typical M-Fly aircraft's flight conditions, namely the Reynolds number and advance ratio. Table 1 shows all relevant parameters used in designing the experiment that yielded the results presented in this document. To perform the experiment, we set the wind tunnel speed to 54.7 ft/s and collected lift and drag data for a sweep on angles of attack (AoA). We ran the motor at full throttle during the entire period that we took measurements. Once all measurements for a given spanwise location were recorded, we moved the motor spanwise using an integrated lead screw mechanism in the test wing, where we repeated the AoA sweep. This was done for ten spanwise locations covering approximately 65% of the test wing.

Experimental Parameters	**Value**
Reynolds number	400,000
Advance ratio	0.2
Airfoil	CH10
Wing span	4 ft
Wing chord	1.15 ft
Propeller	Right handed 14 x 8.5E APC
Propeller speed	9200 RPM
Wind tunnel speed	54.7 ft/s

Table 1 Parameters used in experiment match M-Fly flight conditions.

III. Criteria

To guide the design, build, and test process for investigating the benefits of wing-mounted propellers, two criteria were used to assess all findings and results: effectiveness and practicality.

A. Effectiveness

The most important criterion for the propeller-wing combination is effectiveness, which was determined by the change in aerodynamic performance of the wing with a propeller compared to a base wing with no propeller. Understanding the extent at which a propeller-wing combination affects the vehicle was important as increased aerodynamic performance directly translates to a higher competition score for M-Fly. This was measured by the change in the lift and drag forces acting on the wing for each propeller-wing combination. These forces were non-dimensionalized to create drag

polars of C_L vs C_D for each spanwise location to summarize our results. Aerodynamic performance increases in these drag polars are clearly shown as curves closer to the ordinate, allowing M-Fly to quantitatively assess the effectiveness of having a propeller on the wing of an aircraft. Plots showing C_L/C_D as functions of spanwise location are also used to directly compare performance at constant AoA and observe general trends.

B. Practicality

With regard to our M-Fly sponsor, one of the main deliverables of this study is to provide a suggested spanwise location for future M-Fly dual-motor designs. However, it is important to consider the practical constraints that a typical M-Fly aircraft design must satisfy.

1. Tip Stikes

One potentially dangerous scenario on takeoff or landing is the aircraft rolling to one side and the wingtip striking the ground. If the propeller strikes before the wingtip, the propeller can break and create a hazard for onlookers in the aircraft's vicinity. Thus, a practical design must place the propeller such that it does not impinge on the aircraft's safe tip-over angle. This can be visualized in Figure 1, showing that the wingtip will contact the ground before the propeller on M-Fly's MX-6 aircraft.

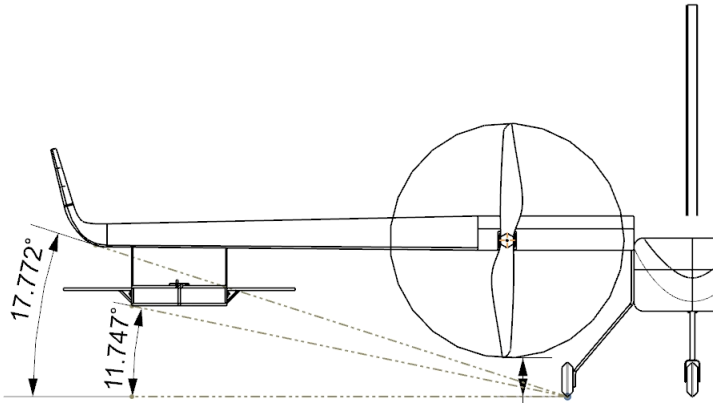

Fig. 1 Tip-over angle of M-Fly's MX-6 shows wingtip would strike ground before propeller.

2. Structural Weight

The second practicality criteria concerns structural weight of the wing. A practical design must increase the lift of the aircraft by more than it increases the weight of the wing due to additional structural reinforcement. Violating this constraint would mean that a design negates its own performance benefits and is not useful for the team. This is most apparent in designs that place the propeller far out on the span and would necessitate significantly extending the wing spar or adding new internal structures to the wing.

The sub-criteria mentioned above are highly dependent on geometry and design choices specific to each aircraft, so it is impossible for us to evaluate them in the scope of this project. However, they

should be strongly considered if M-Fly chooses to use the results of this project when designing future aircraft.

IV. Design

The design of our project, from literature review to system validation, was driven by matching M-Fly flight conditions through scaling nondimensional parameters to a model that could be tested within the University's facilities. Specifically, we determined that our test wing and propeller should match the Reynolds number and advance ratio of a typical M-Fly aircraft, and that these conditions could be achieved within the University's 5- by 7-foot wind tunnel facility. This physical model could then be used to verify a CFD model of the wing with varying propeller placements. In addition, the constraints of the course required that our test wing could not exceed a budget of $400.00 and has to be manufacturable and testable in a time-frame of 10 weeks.

A. Matching Flight Conditions

To draw reasonable correlations between M-Fly aircraft in-flight and our tests, we matched two key nondimensional coefficients between each condition: the Reynolds number (Re) and the advance ratio (J). Formulas for the Reynolds number and advance ratio can be seen in Equations 1 and 2.

$$Re = \frac{\rho U_\infty L}{\mu} \tag{1}$$

$$J = \frac{U_\infty}{nD} \tag{2}$$

As M-Fly aircraft typically operate below 100 ft, we considered the air density (ρ) and viscosity (μ) to be constant. The remaining variables, including freestream airspeed (U_∞), propeller diameter (D), wing chord length (L), and rotation rate (n) are all fixed throughout the study in both the physical design of the test-wing and the test conditions. From Table 1, typical M-Fly aircraft have a cruise Reynolds number of 400,000 and an advance ratio of 0.2 – both of which are attainable conditions in the University's 5- by 7-foot wind tunnel facility.

B. Propeller and Wing Sizing

From matching M-Fly flight conditions to our model, we chose a 14- by 8.5-inch diameter propeller with an untapered wing measuring 4 feet in span and a chord length of 1.15 feet, giving an aspect ratio of 6.95. Our wing design was constrained by the dimensions and mounting configuration of the University's 5- by 7-foot wind tunnel facility. The wind tunnel's load balance setup lies beneath the test section and can only support a vertical mounting configuration; as such, our test wing was constrained to the 5 foot height of the wind tunnel test section. To allow for space between our wingtip and the wind tunnel ceiling for wingtip effects, we chose a 4-foot wing span for our wing model. We decided on an untapered wing for ease of manufacturability, and incorporating a typical M-Fly wing aspect ratio of 6.95, our wing had a chord length of 1.15 feet. The equivalent airspeed at this chord length and the M-Fly Reynolds number of 400,000 is 54.7 ft/s, which is attainable in the University's wind tunnel facilities. With the airspeed fixed in our advance ratio equation, we sized our propeller to match the advance ratio of 0.2, and compared possible propeller diameter sizes with rotation rates, as shown in Figure 2.

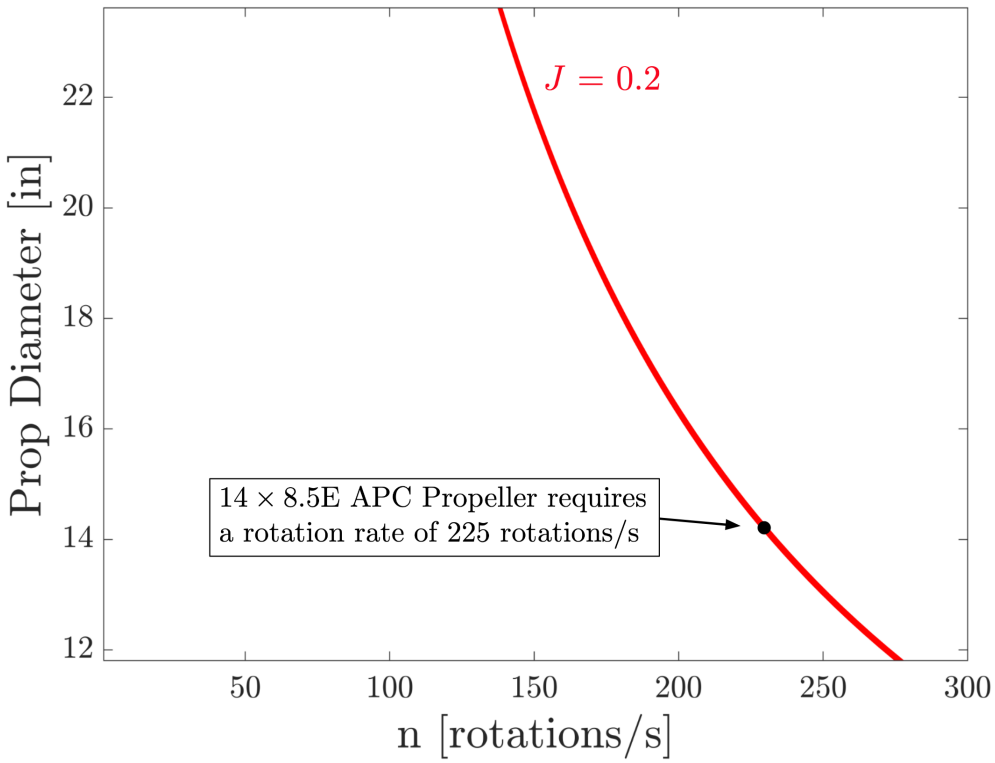

Fig. 2 The range of feasible propeller rotation speeds and diameters for matching the advance ratio of 0.2 are highlighted in red.

From this trade study, we selected a 14- by 8.5-inch diameter propeller with a rotation rate of 225 rotations per second, as this size propeller is readily available and the rotation rate is within the operational limits of a Dual Leopard 4250-7T propeller motor provided by M-Fly.

C. Test Wing Design

We carried out the detailed design of our testing rig in SolidWorks. Our rig design allows the spanwise position of the motor to be adjusted with the wind tunnel through a 12V DC motor powering an integrated lead screw and rail system embedded within the wing spar structure, as shown in Figure 3. Both of the rails used in the system are covered with rubber strips to minimize flow blockage and ensure smooth air flow under the wing. A detailed bill of materials for our test-wing design can be found in Appendix A.

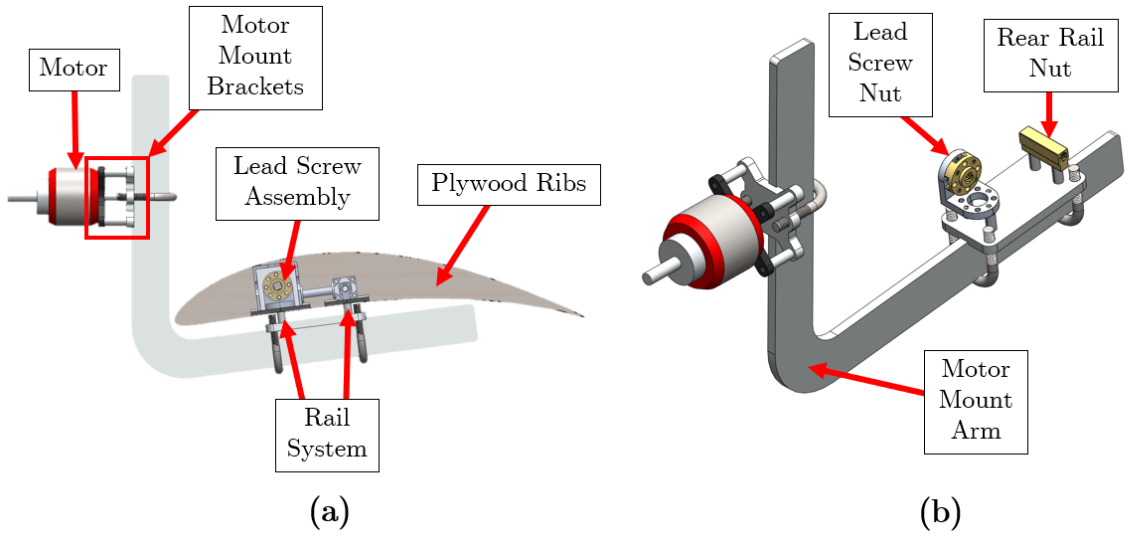

Fig. 3 (a) Cross-section view and (b) isometric view of our rig design illustrating the wing structure and integrated lead screw mechanism.

We designed the rig such that it also incorporates vertical and streamwise degrees of freedom for our motor which are adjustable through U-shaped bolts. Altogether, our rig design leaves the top surface of the wing clear and reduces the impact of the rig on our wind tunnel results.

To account for the vertical mounting configuration in the 5- by 7-foot wind tunnel, we designed a connecting rod on the root of our test wing that attaches to the vertical mount at the floor of the wind tunnel, shown in Figure 4.

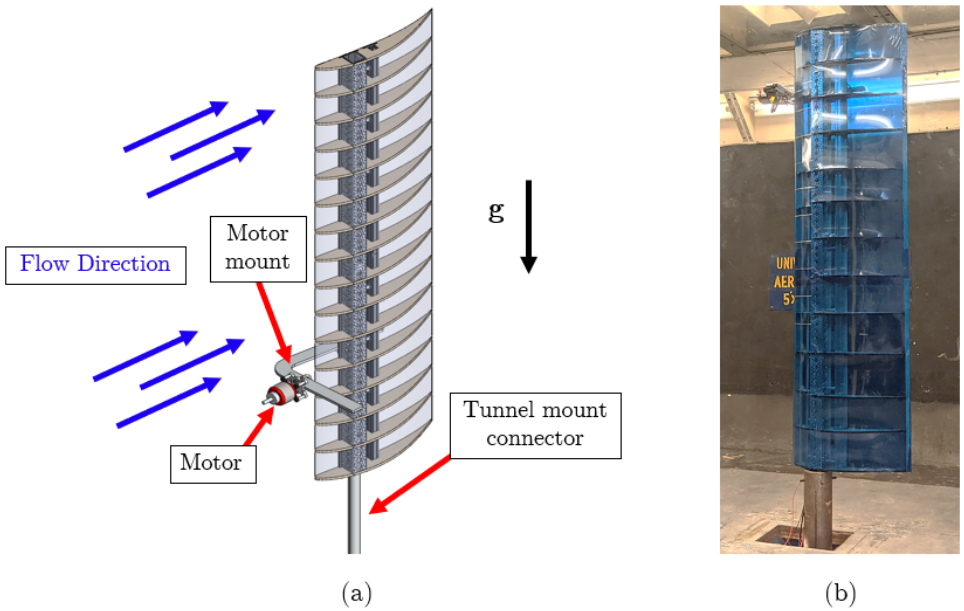

Fig. 4 (a) Test rig layout in CAD, (b) physical test rig layout in the 5- by 7-foot wind tunnel facility.

As we were not constrained on weight for our wing model, we selected 6061 Aluminum as the material for our wing spar and rail system because of its high strength and availability. Additionally, our wing ribs consist of 1/4-inch plywood, chosen for its availability and ease of manufacturing with a laser cutter.

D. Test Wing Fabrication

Our test wing design utilized traditional machining methods for certain components. The milling machines at the Wilson Student Team Project Center (WSTPC) were used to carve out a channel in a mounting plate, and a water-jet machine was used to cut several parts from an aluminum plate, including a bracket arm that supports the motor and propeller. We water-jetted parts at the University of Michigan Mechanical Engineering x50 machine shop through one of our team members. Detailed dimension drawings for these components can be found in Appendix B.

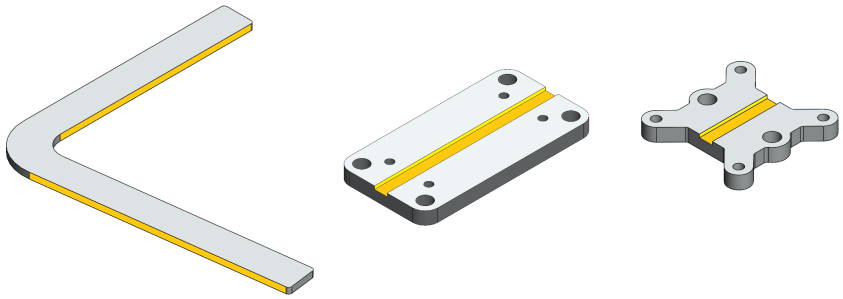

Fig. 5 (Left) Test rig motor mount arm, (middle) rig joiner plate, and (right) rig motor plate that were cut on the water-jet machine. Surfaces that required additional machining through the mills are highlighted in yellow.

We utilized a CNC laser cutter in the University's Aerospace Department to precisely cut out the wing rib profiles. The use of this laser cutter allowed the team to rapidly make minor corrections to the ribs and auxiliary wood components in the wing section. We purchased most other components, such as the aluminum spars, rails, and lead screw mechanism components to ensure compatibility and satisfy time constraints.

We assembled the main structure of our wing through attaching our wing ribs, aluminum spar and rail system together using epoxy and screws for structural integrity and stiffness. We then integrated a lead screw mechanism and attached a Servocity 52RPM 12V DC motor to spin the lead screw that moves the motor mount bracket along the wing span. We determined this motor to be sufficient for our mechanism, with our operating conditions falling within the motor's torque limit of 292 oz-in and power limit of 60W. After interfacing the motor and lead screw mechanism into the wing structure, we covered the open gaps in the rail system with rubber flaps to minimize flow blockage on the underside of the wing. Once we attached the motor and motor mount bracket to the rail system, we applied a thin Ultracote layer over the entire wing to form the wing's external skin. We lubricated all moving components with grease to ensure that the mechanism did not jam mid-test.

E. CFD Model Setup and Design

For our CFD model, we recreated the University's 5- by 7-foot wind tunnel facility with a to-scale computational recreation in Star-CCM+ software (Figure 6). Specifically, we modeled the 25-foot constant-area test section of the wind tunnel. From there, we recreated our test-wing and inserted it within the tunnel at the same location as the physical setup. We modeled the facility walls and the wing as no-slip conditions to reflect a physical barrier. The inlet and the outlet of the facility were declared as a velocity inlet and pressure outlet, respectively. We specified the velocity inlet to be 54.7 ft/s.

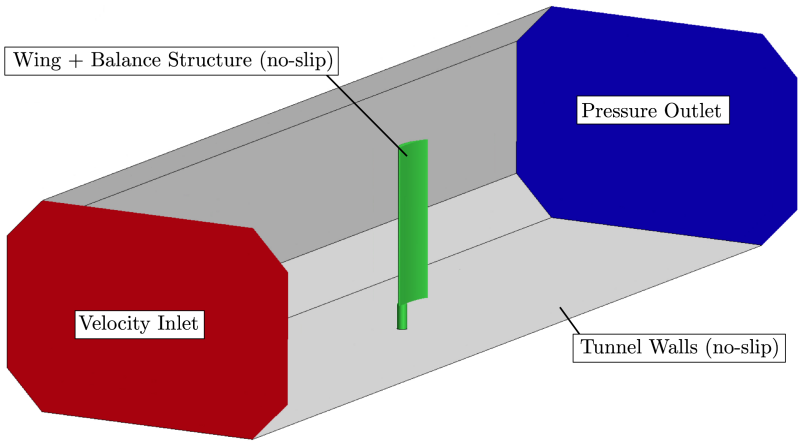

Fig. 6 CFD simulation diagram of the University's 5- by 7-foot facility. Surfaces are colored according to their boundary condition.

Seen in Figure 7, we started with a base wing case (propeller detached) at an AoA of $\alpha = 8°$. The simulation was run until all residuals had reached at least $O(10^{-3})$, and values of lift and drag had reached steady state, before moving on to other values of α in the range of 0° to 10°. An example of this convergence criteria can be seen in Appendix C.

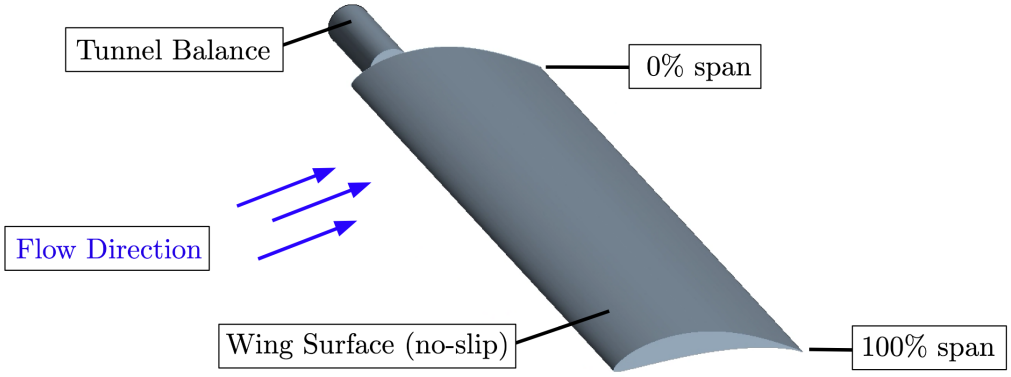

Fig. 7 CFD model of the base wing configuration in Star-CCM+, with the propeller detached from the wing. AoA was varied by 2° increments in the range of 0° to 10°.

We used Star-CCM+'s Virtual Disk model to simulate the propeller in CFD. This required us to specify the propeller's performance across different conditions, specifically, the thrust coefficient (C_t), torque coefficient (C_q), and propeller efficiency (η) specified as functions of advance ratio. Equations for these parameters can be found in Equations 3 through 5. These functions were found as part of 2- by 2-foot wind tunnel testing in our Phase I report.

$$C_t = \frac{T}{\rho n^2 D^4} \tag{3}$$

$$C_q = \frac{Q}{\rho n^2 D^5} \tag{4}$$

$$\eta = J\frac{C_t}{2\pi C_q} \tag{5}$$

Seen in Figure 8, we ran a simulation identical to the base wing case with the Virtual Disk model in place of our physical propeller. Again, we ran each simulation until residuals were below $O(10^{-3})$, and values of lift and drag reached steady state, before moving on to other values of α.

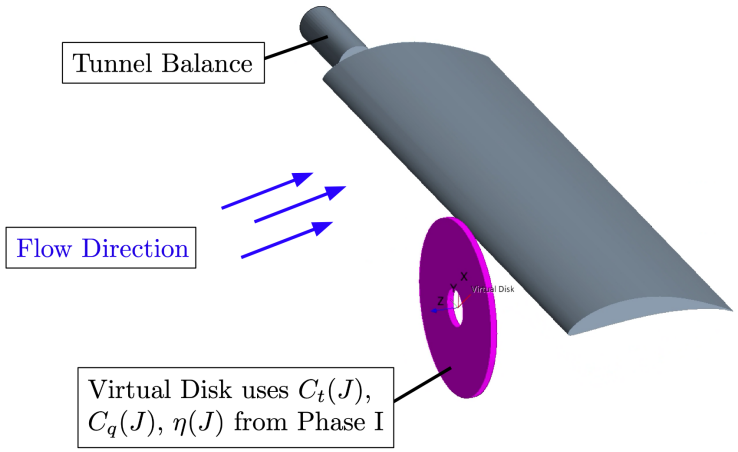

Fig. 8 CFD model of the full test wing configuration in Star-CCM+ with the Virtual Disk model. AoA was varied by 2° increments in the range of 0° to 10°.

V. Support

The following section discusses support for each of the criteria based on the data collected.

A. Support for Effectiveness

There are multiple metrics to consider when analyzing the effectiveness of any given design. To ensure that the effectiveness of our results can be extracted in a quantified fashion, the team collected full drag polars with the motor bracket at multiple spanwise locations with (1) the propeller at full throttle and (2) with the propeller entirely removed. The second case allows us to capture the baseline performance of the wing for a given configuration without the influence of a propeller,

allowing for comparison between our computational and experimental models. Integral to these comparisons is the use of nondimensional coefficients, namely the lift coefficient (Equation 6) and drag coefficient (Equation 7). Formulas for these coefficients can be found below, where L is the lift force, D is the drag force, ρ is the air density, U_∞ is the freestream velocity, and S is the wing reference area.

$$C_L = \frac{L}{\frac{1}{2}\rho {U_\infty}^2 S} \tag{6}$$

$$C_D = \frac{D}{\frac{1}{2}\rho {U_\infty}^2 S} \tag{7}$$

Starting with the base wing, we performed a comparison between our CFD simulations and Athena Vortex Lattice (AVL) – a low-fidelity inviscid flow solver. As shown in Figure 9, our CFD simulation of the base wing followed the same trends seen in AVL, verifying that our base wing CFD model can be trusted.

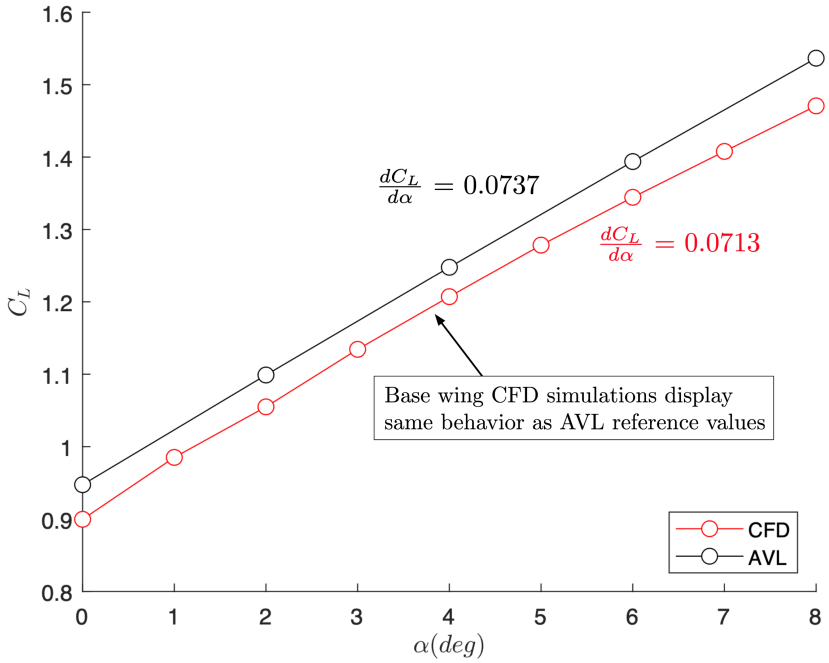

Fig. 9 Base wing (propeller detached) comparison of CFD vs AVL results. Base wing CFD simulations are validated as they closely follow the inviscid approximation of AVL.

Additionally, using measurements from our 5- by 7-foot tunnel experiment, we created drag polars of the base wing with the motor mount at varying positions. The results of this experiement can be seen in Figure 10. Clearly, we can see that the spanwise placement of the motor mount has minimal effect on the aerodynamic performance of the wing as the drag polars are nearly identical between runs. This verifies that any performance changes we observe with the propeller attached can be attributed purely due to the propeller, and not our test wing structure.

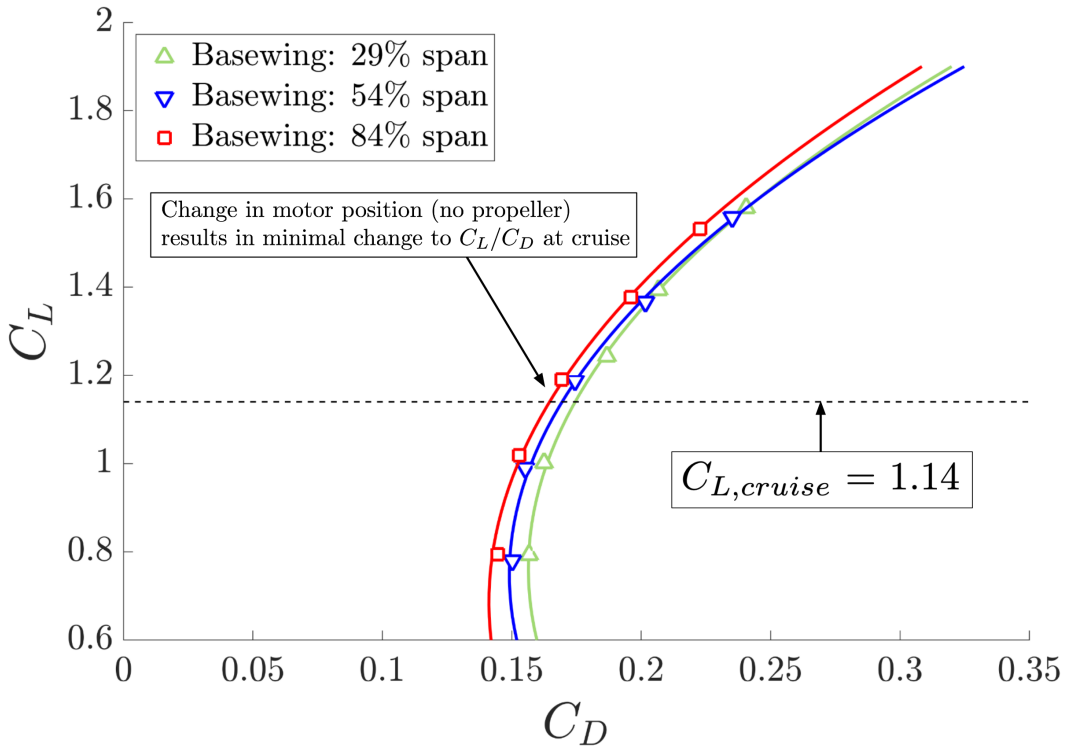

Fig. 10 Experimental drag polars for 3 spanwise locations on the base wing (propeller detached). Aerodynamic performance is not dependant on the spanwise placement of the motor mounting structure.

Once the baseline data has been examined and our CFD model has been validated, we compared it to the data with the propeller running. Focusing on a M-Fly cruise condition of $\alpha_{cruise} = 8°$, we calculated the wing lift-to-drag ratio, defined as C_L/C_D, for each spanwise position of the propeller. Values of C_L/C_D were also extracted from our CFD Virtual Disk simulations and are plotted against our experimental data. Results of this comparison can be found in Figure 11.

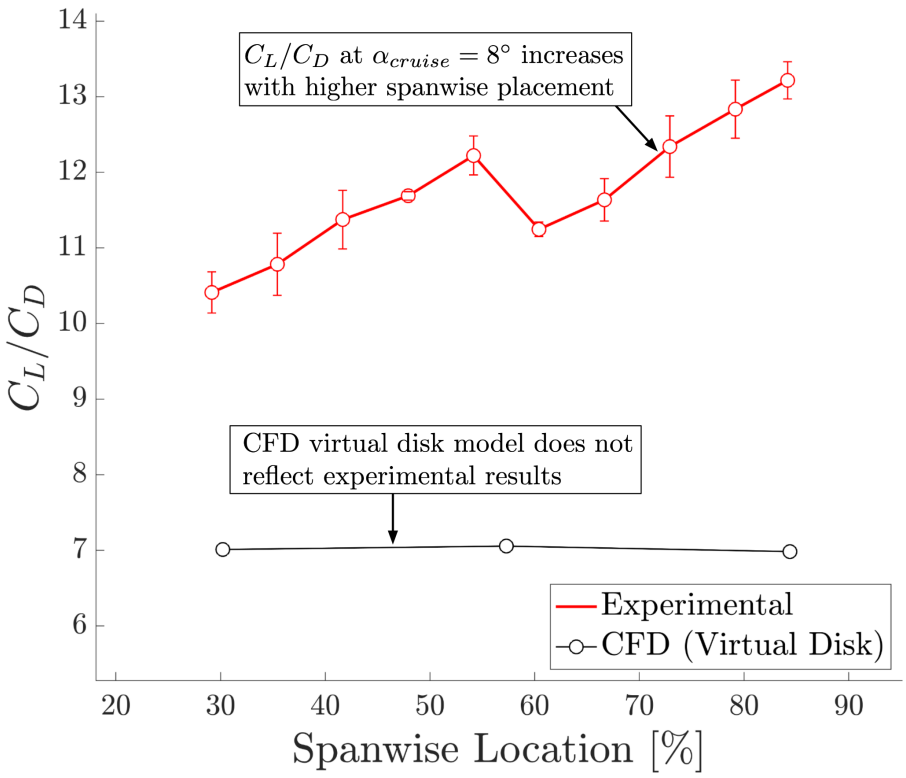

Fig. 11 Comparison of experimental (5- by 7-foot facility) and computational (Star-CCM+) results. The proposed Virtual Disk model does not follow the trends seen in physical experiments.

Here, our experimental results show a trend of increasing C_L/C_D with increasing spanwise placement of our propeller. However, our Virtual Disk model did not seem to support this conclusion. This discrepancy suggests that our Virtual Disk computational setup is a flawed representation of a propeller and that its results should not be trusted for the duration of this study.

To further investigate the changes in C_L/C_D, we again used our experimental results from the 5- by 7-foot facility to create drag polars for different spanwise placements of our propeller. Seen in Figure 12, it is clear that a higher spanwise placement results in a leftward shift of the wing drag polar. This has the overall effect of the aircraft experiencing lower drag for a given amount of lift. More specifically, we see that the 84% spanwise configuration has resulted in a change of $\Delta C_D = 0.1$ for a typical M-Fly cruise condition compared to the basewing – a large improvement.

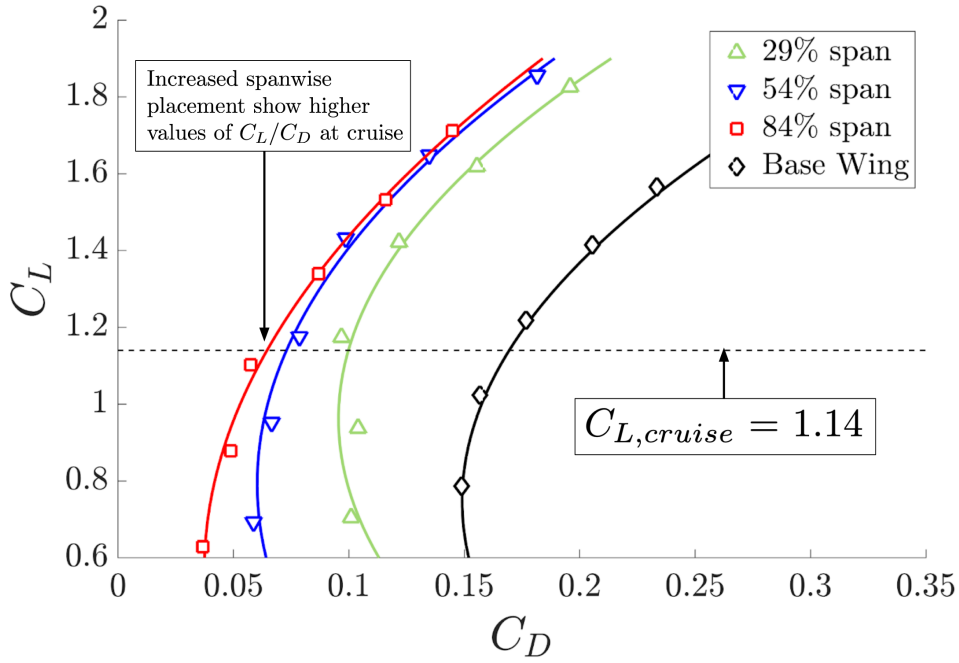

Fig. 12 Experimental drag polars for 3 spanwise locations for the complete test wing (propeller attached and active). Wing C_L/C_D is directly related to propeller spanwise placement.

To summarize, we observed the following trends in the data:

1) Base wing CFD models follow expected performances, but deviate when the Virtual Disk model is introduced (Figure 11).
2) With the propeller detached, the location of the motor mounting structure has a minimal effect on the performance of the wing (Figure 10).
3) With the propeller attached and active, the C_L/C_D of the test wing is directly related to the spanwise position of the propeller (Figure 11).
4) A higher spanwise placement of the propeller shifted the drag polar curves to the left on the C_L vs C_D axis when compared to the base wing with no propeller (Figure 12).

The impact of these trends and follow-on conclusions will be discussed in Section VI.

B. Support for Practicality

The support for practicality is much simpler to analyze than support for effectiveness. Where effectiveness is considering multiple objective functions, practicality looks at the satisfaction of two requirements: minimum prop-strike angle and required wing structure.

It is important to note, however, that both requirements are highly plane-dependent. In particular, they depend on the configuration and construction materials of the aircraft. For example, an aircraft with a low-wing configuration will have less clearance between the wing and the ground compared to a high-wing configuration, and thus will not be able to accommodate propellers at far spanwise placements. If a plane was tasked with carrying payloads beneath its wings, then wing-mounted propellers would likely decrease the space available to payloads and potentially hinder the payload

capacity of the aircraft. For these reasons, it is difficult to state many quantified requirements for a wing-mounted propeller design to be practical in the eyes of its designers. When deciding upon the practicality of a potential wing-mounted design, we suggest that M-Fly should holistically consider:

1) Clearance distances during taxi between a wing mounted propeller and the ground.
2) Added structural weight of a wing with a wing-mounted propeller and motor system.
3) Negative aerodynamic effects of having wing-mounted payloads placed behind the wake of a propeller.
4) Flight line danger of wingtip/propeller strikes during takeoff and landing.

If a potential spanwise placement of a propeller is seen to violate these conditions in the eyes of the aircraft engineers, it is likely that the proposed design will not be feasible for M-Fly's mission goals.

VI. Conclusions and Alternatives

Our team drew the following conclusions regarding our work and alternatives for future work.

A. Conclusions

From the results of our study, we conclude that a wing-mounted propeller configuration is beneficial to the performance of M-Fly aircraft as long as it satisfies the practicality criteria. Wind tunnel testing indicated that propeller-wing interaction generally improved the lift-to-drag ratio of the wing over the base configuration, with increasing benefits as the propeller spanwise position approached the wingtip (farther from the centerline). Though performance unexpectedly decreased near the center of the wing, all investigated spanwise propeller locations produced a net increase in wing lift-to-drag ratio. As such, our team recommends the use of the wing-mounted dual-propeller configuration for future M-Fly aircraft.

B. Alternatives and Future Recommendations

Many of the difficulties that the team encountered during testing of the wing rig could have been mitigated with alternate approaches to rig design. In particular, the inclusion of a wing root end-plate may have provided a better approximation of the propeller interaction with the fuselage of a typical M-Fly aircraft.

Additionally, it is important to note that our computational Virtual Disk model in Star-CCM+ did not result in the same trends seen in physical experimentation. The Virtual Disk model is a novel approach to our team, and we were thus unsure as to whether it would accurately model a realistic interaction between a wing and a propeller. The stark contrast in C_L/C_D values, as discussed in Section V.A, suggest that the Virtual Disk model is unsuitable for this type of flow. We recommend future teams investigate the use of rotating reference frames in Star-CCM+ to accurately model an aircraft propeller.

C. Omissions, Errors, and Limitations

1. Omissions

Due to time and budget limitations, we have chosen not to investigate certain parameters identified in our preliminary literature review. These include propeller angle of incidence, propeller stream-wise position, and locations of the propeller behind the wing. The decision to focus on propeller spanwise position was based on our expectation that spanwise location would have the greatest impact on wing lift and drag properties. However, we expect that varying these additional parameters would still have a measurable impact on aircraft performance. Thus, we recommend that future teams who are interested in this subject investigate these alternative propeller locations.

Additionally, our study investigated only one combination of Reynolds and Mach number, simulating typical cruise conditions for M-Fly aircraft. Our team made the decision to exclusively target cruise flight due to M-Fly aircraft typically spending the most time in this phase, meaning that benefits to performance at cruise would have the greatest impact to the mission. Nonetheless, we recommend that future teams also investigate other important flight regimes, in particular takeoff and landing, to gain a more comprehensive understanding of the effect of wing-propeller interactions on an aircraft as a whole.

2. Errors

We are still concerned with the characterization of our propeller obtained in Phase I of our project. The constrained propeller effect described by Glauert [7] caused our experimental propeller characterization to be misaligned with the propeller manufacturer's data across most of our entire test range. However, our results aligned well with the reported performance data at low speeds and only deviated significantly at the high end of the range. This trend gave us some confidence in our results, which we believed to be valid at our final operating point. Beyond Phase I, Phase II testing presented a number of potential sources of error. We aimed to keep the 5- by 7-foot wind tunnel at speed for as long as possible during testing, which limited our ability to re-zero the balance after testing each spanwise location. However, any drift is the system should have been minimized by the fact that we tested the full range of spanwise locations twice, once going towards the wingtip and once going towards the wing root. Further, it was difficult to set the wind tunnel to exactly the desired speed of 54 ft/s, causing our data points to have slight variations of ± 1.5 ft/s from the design speed. Finally, all motor RPM values used were reliant on the accuracy of our static testing and were not exact.

3. Limitations

A major limitation of our study was the geometry of the wind tunnel. Our original design for the wing testing rig specified that the inboard end of our test wing would be located flush with the floor of the wind tunnel to simulate the effect of the fuselage wall on the flow. However, during testing it was discovered that the height of the load balance prevented the wing root from being placed any lower than 8 inches from the wind tunnel floor. As such, we were unable to fully capture the effects of the interaction between the propeller and tunnel floor during our time in the wind tunnel, limiting the applicability of our results to M-Fly aircraft. Future teams should consider using a ground-plane box to solve this issue.

Due to time constraints, our team was also limited in the resolution of our study for both CFD simulation and wind tunnel testing. To finish testing within the two days allotted to our team in the 5- by 7- foot wind tunnel, we marked and took measurements at just ten discrete stations along the span of the wing. We would recommend that any teams interested in our results might attempt to recreate our results with higher-fidelity testing at more discrete stations on a test wing.

VII. Management Plan

While the primary goal of the project was to gather useful data and extrapolate their impact to M-Fly, it was also important that the team did so while staying on-budget and on-schedule.

A. Budget

The majority of the budget for this project was allocated towards materials for the test wing, primarily consisting of plywood, aluminum parts, and fasteners as seen in Table 2. The team soon realized after purchasing the plywood that the plywood had been over-budgeted, and we needed significantly less than originally thought. While the test wing ended up being fairly expensive to construct at $639.02, the team only needed to spend $322.10. This is because M-Fly generously sponsored the power supply and loaned it to the team for this project. The power supply was a last-minute addition to the test wing, and the 5- by 7-foot wind tunnel testing would not have been carried out in a timely fashion had we relied on Li-Po batteries to power the motor instead. The two differences between the initial and final budgets comes from the addition of the power supply and the decreased wind tunnel test time; this generated an increase of $316.92 on the test wing subtotal and a decrease of $2,341.50 on the wind tunnel budget. Even without this decrease in wind tunnel testing, our contingency would have accommodated the added cost of the power supply.

Aside from the previously mentioned components, the team purchased several small electronics and auxiliary materials such as grease to keep the test wing mechanism lubricated during testing. These brought the total material cost to $357.13 and is within the $400.00 budget for the course. Labor, wind tunnel time, and overhead/contingency are the largest line items on the budget; however, they are purely theoretical costs and were never realized by the team.

A full Bill of Materials with component details can be found in Appendix A. The budget below has been condensed for the sake of brevity.

Table 2 Cost breakdown by component.

Category	Item	Unit Cost ($)	Qty.	Est. Cost ($)	Total Cost ($)
Test Wing	24” x 36” x 1/4” Plywood	12.00	5	60.00	60.00
	Ultracote ™	15.00	1	15.00	15.00
	Aluminum Sheet	27.95	1	29.95	29.95
	Rubber Strip	14.00	1	14.00	14.00
	U-Bolts	3.58	1	3.58	3.58
	Slot Washers	2.69	1	2.69	2.69
	U-Channel	34.99	1	34.99	34.99
	Open X-Rail	14.29	1	14.29	14.29
	0.5” Al. Spacer	1.49	1	1.49	1.49
	0.75” Al. Spacer	1.69	2	3.38	3.38
	1.0” Al. Spacer	1.89	2	3.78	3.78
	8mm Lead Screw	20.99	1	20.99	20.99
	8mm Lead Screw Nut	7.99	1	7.99	7.99
	90° Pattern Mount	4.99	1	4.99	4.99
	52 RPM DC Motor	27.99	1	27.99	27.99
	Shaft Coupler	8.39	1	8.39	8.39
	Clamping Mounts	5.99	3	17.97	17.97
	16” Al. Tubing	6.69	1	6.69	6.69
	Lead Screw Nut	12.99	1	12.99	12.99
	Pillow Block	7.99	2	15.98	15.98
	X-Rail Nut	4.99	2	9.98	9.98
	Lead Screw Clamp	4.99	1	4.99	4.99
	Power Supply	316.92	1	0.00	316.92
			Subtotal	**322.10**	**639.02**
Materials	PTFE Grease	9.79	1	9.79	9.79
	Screws (various)	9.27	1	9.27	9.27
	Two-part Epoxy	15.97	1	15.97	15.97
			Subtotal	**35.03**	**35.03**
Labor	Engineer	40/hour	800	32,000	32,000
Labor	Technician	40/hour	12	480	480
Wind Tunnel	Rental	315/hour	5.9	4,200	1,858.5
Overhead	-	50% of subtots.	-	18,278.56	18,437.02
Contingency	-	10% of subtots.	-	3,655.71	-
			TOTAL	**58,971.40**	**53,449.57**

B. Schedule

The schedule for this project had to be adjusted numerous times during the first half of the semester due to major redesigns of the test wing. The original plan was to manually remove the propeller/motor subassembly and reattach it at various spanwise locations. However, the team's advisors suggested we design a more automated approach as the original design would require powering off the wind tunnel between the collection of each drag polar. Thus, the team spent extra time designing the wing and motor rig and opted to make a more concentrated effort in the manufacturing and testing phases. For example, wind tunnel testing was originally planned to span a 3 week period, and instead only took two days. It should also be noted that AERO405 teams are only promised two days in the 5- by 7-foot tunnel, and this new schedule better reflected this constraint.

Beyond the major testing campaign, the team conducted smaller tests with the 2- by 2-foot wind tunnel throughout the project. These were used to gather data for the CFD simulations, predict the propeller motor battery life for the 5- by 7-foot testing, and locate the maximum achievable motor RPM. Routine thrust testing built confidence in the propulsion system and gave the team ample practice troubleshooting motor problems in preparation for the 5- by 7-foot tunnel testing. Finally, the team completed extensive testing on the lead screw mechanism of the test wing to ensure the lead screw DC motor was able to move along the wing during testing. This revealed minor problems in the mechanism design, which were resolved prior to the final test.

As most engineers know, even with rigorous testing things can still go wrong. Near the end of the first day of 5- by 7-foot tunnel testing, the coupler attaching the DC motor to the lead screw failed catastrophically. However, the team was able to work together to make quick modifications to the wing and complete the test before the wind tunnel technician had to leave for the day.

The Gantt chart in Figure 13 shows the project schedule in two states: planned and executed. The first instance of each task represents its planned timeline (denoted with a "(P)"), and the coloring reflects the outcome: green = on-time, red = late, and blue = ahead of schedule. The second instance of each task shows its actual execution and is denoted with an "(E)". While the majority of the tasks in the middle of the project were completed late due to the test wing rig redesign, the abbreviated schedule at the end of the semester allowed the team to finish on-time. All major milestones are shown at the bottom of the chart and were completed on-time.

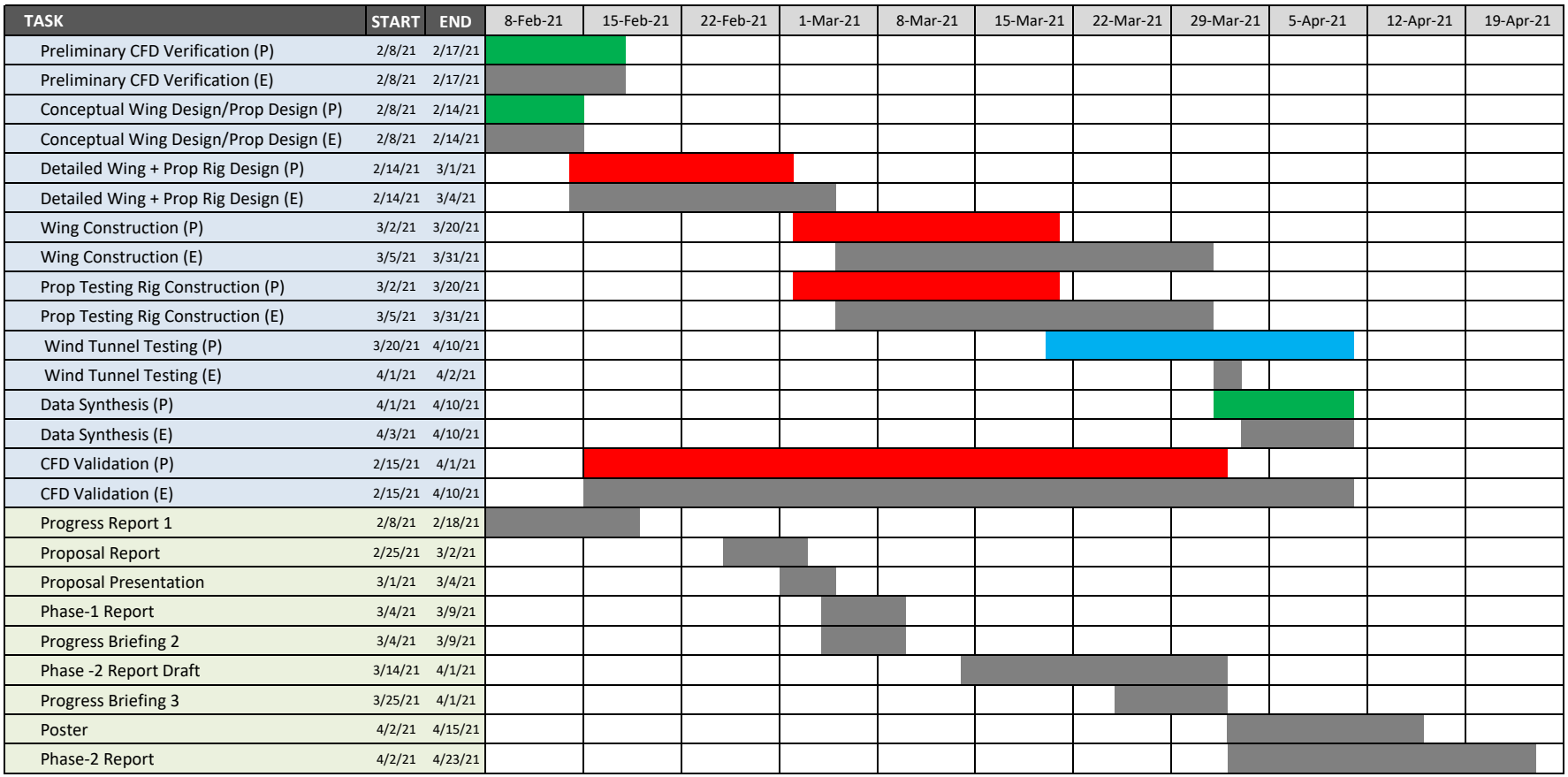

Fig. 13 Project schedule. Planned timeline is denoted with "(P)", executed is denoted with "(E)". Green = completed on-time, red = late, blue = completed ahead of schedule.

References

[1] Wood, D. H. (1932). Tests of nacelle-propeller combinations in various positions with reference to wings. Part I : Thick wing-N.A.C.A. cowled nacelle-tractor propeller. *18th Annual Report of the National Advisory Committee for Aeronautics,* 277-305. Retrieved March 2, 2021, from https://digital.library.unt.edu/ark:/67531/metadc66072/:.

[2] Wood, D. H. (1936). Engine Nacelles and Propellers and Airplane Performance. *SAE Technical Paper Series.* doi:10.4271/360111

[3] Veldhuis, L.L.M., "Review of Propeller-Wing Aerodynamic Interference," *24th International Congress of the Aeronautical Sciences,* August 2004. http://icas.org/ICAS_ARCHIVE/ICAS2004/PAPERS/065.PDF

[4] Gholami, B., "Ship Propeller Transient Flow Simulation," SimScale GmbH, December 2015.

[5] Ma, S., Ming, Q., Wang, J., Miao, T., & Jiang, X., "Application of CFD in Slipstream Effect on Propeller Aircraft Research," *Acta Aeronautica et Astronautica Sinica,* Vol. 40, No. 4, 2019. http://hkxb.buaa.edu.cn/EN/Y2019/V40/I4/622365

[6] Gilbert, M., Abibal, J., Hill, R., Piscoran, R., & Wallace, K. (n.d.). *Increasing Maximum Lift of Remote-Controlled Aircraft with Wing-Mounted Propellers* (Tech.).

[7] Glauert, H. (1983). The Elements of Aerofoil and Airscrew Theory (Cambridge Science Classics). Cambridge: Cambridge University Press. doi:10.1017/CBO9780511574481

A. Test Wing Bill of Materials

Category	Qty.	Component	Supplier
Main Structure	13	Lasercut Wing Ribs	Plywood stock
	4	1/16” x 1/2” x 24” Trailing Edge Strips	Balsa stock
	2	1/2” x 3/4” x 24” Leading Edge Stock	Balsa stock
	1	1/4” x 1/4” x 48” Ply Stringer	Plywood stock
	1	48"-Long U-Channel Bar (main spar)	Servocity
	1	Ultracote™ plastic film	Hangar 9
	1	4.5oz 2-Part Quik-Cure Clear Epoxy	Bob Smith Industries
	1	8oz Insta-Cure Cyanoacrylate Glue	Bob Smith Industries
Primary Rail System	1	37.4” 8mm Diameter Lead Screw, 2mm Pitch	Servocity
	1	8mm Diameter Lead Screw Nut, 2mm Pitch	Servocity
	1	90° 0.77” Pattern Mount	Servocity
	1	52 RPM 12V DC Planetary Gear Motor	Servocity
	1	4mm to 8mm Flex Shaft Coupler	Xnrtop, Inc.
	2	1” Side Tapped Clamping Mount	Servocity
	1	22mm Side Tapped Clamping Mount	Servocity
	1	3504 Series Lead Screw Clamping Collar	Servocity
	1	8mm Bore Side Tapped Pillow Block	Servocity
	15	6-32 x 1-3/8” Socket Head Machine Screw	Servocity
	2	1/8” x 1/2” x 10’ Neoprene Rubber Strip	Seal Innovations, Inc.
Secondary Rail System	2	24”-Long Open X-Rail (secondary rail spar)	Servocity
	1	6mm Lead Screw Nut for Open X-Rail	Servocity
	10	0.5” Length, 1/4” OD Aluminum Spacer	Servocity
	10	0.75” Length, 1/4” OD Aluminum Spacer	Servocity
	10	1.0” Length, 1/4” OD Aluminum Spacer	Servocity
	15	6-32 x 1/4” Socket Head Machine Screw	Servocity
	15	6-32 x 1” Socket Head Machine Screw	Servocity
	2	585756 X-Rail Nut (4-pack)	Servocity
	50	0.562" OD Slot Washers	McMaster-Carr
	2	1/8” x 1/4” x 10’ Neoprene Rubber Strip	Seal Innovations, Inc.
Mounting Hardware	1	Motor Mount Rig Bottom Arm (waterjet)	6061 Aluminum stock
	1	Motor Mount Rig Motor Plate (waterjet)	6061 Aluminum stock
	1	Motor Mount Rig Joiner Plate (waterjet)	6061 Aluminum stock
	1	1” x 16” Aluminum Tubing	Servocity
	1	1" ID, 1-3/4” Height, 1/4”-20 U-Bolts	McMaster-Carr

B. Engineering Drawings

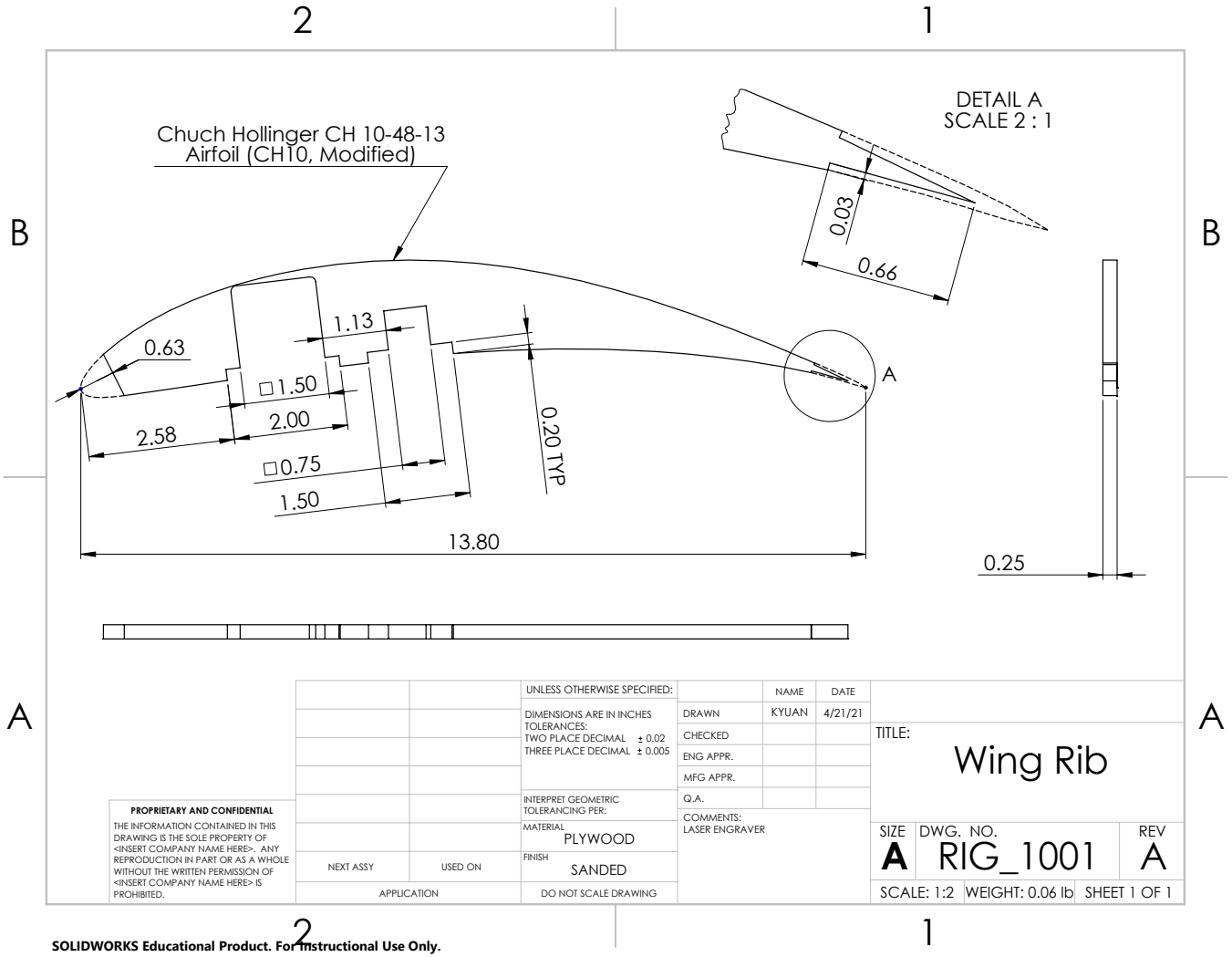

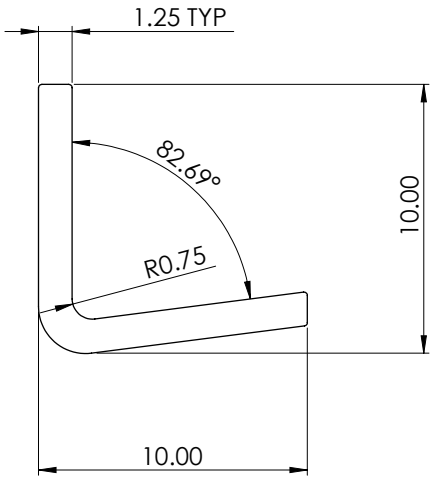

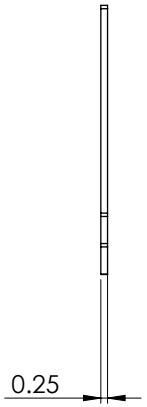

		UNLESS OTHERWISE SPECIFIED:		NAME	DATE
		DIMENSIONS ARE IN INCHES TOLERANCES: ANGULAR: MACH ±0.5deg TWO PLACE DECIMAL ±0.03	DRAWN	KYUAN	3/13/21
			CHECKED	LMART	3/13/21
			ENG APPR.		
			MFG APPR.		
		INTERPRET GEOMETRIC TOLERANCING PER:	Q.A.		
		MATERIAL Aluminum	COMMENTS: WATERJET		
NEXT ASSY	USED ON	FINISH Rough			
APPLICATION		DO NOT SCALE DRAWING			

TITLE:
Rig Top Arm

SIZE	DWG. NO.	REV
A	RIG_1002	A

SCALE: 1:5 | WEIGHT: 0.56 lb | SHEET 1 OF 1

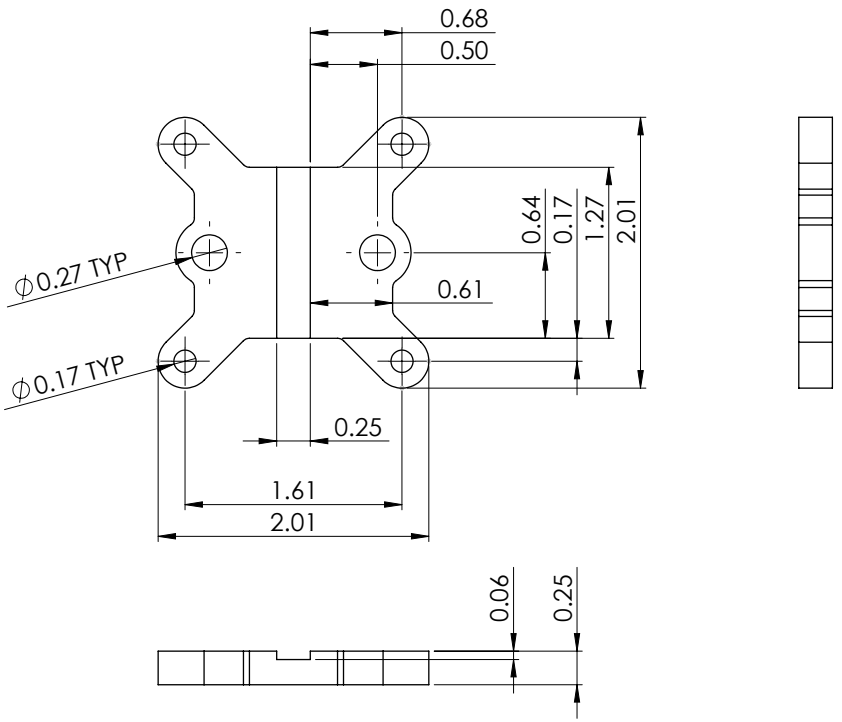

		UNLESS OTHERWISE SPECIFIED:		NAME	DATE
		DIMENSIONS ARE IN INCHES TOLERANCES: ANGULAR: MACH ± 0.5deg TWO PLACE DECIMAL ±0.03	DRAWN	KYUAN	3/14/21
			CHECKED		
			ENG APPR.		
			MFG APPR.		
		INTERPRET GEOMETRIC TOLERANCING PER:	Q.A.		
		MATERIAL Aluminum	COMMENTS: WATERJET		
NEXT ASSY	USED ON	FINISH Rough			
APPLICATION		DO NOT SCALE DRAWING			

TITLE:
Rig Motor Plate

SIZE	DWG. NO.	REV
A	RIG_1003	A

SCALE: 1:1 | WEIGHT: 0.06 lb | SHEET 1 OF 1

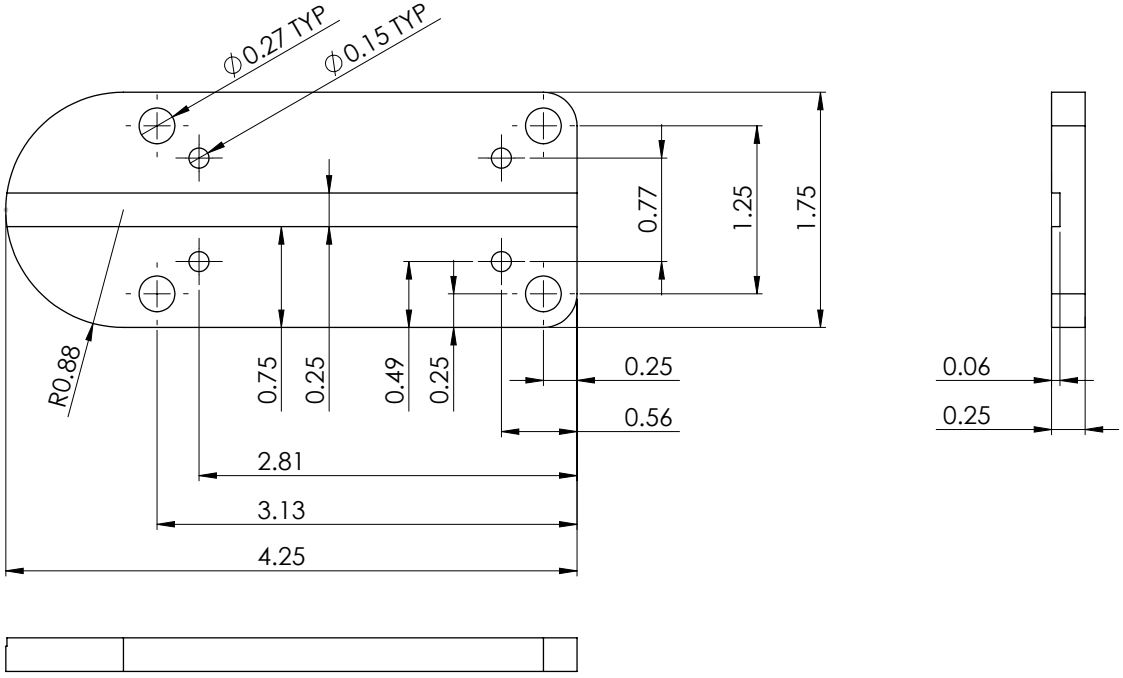

		UNLESS OTHERWISE SPECIFIED:		NAME	DATE
		DIMENSIONS ARE IN INCHES TOLERANCES: ANGULAR: MACH ±0.5deg TWO PLACE DECIMAL ±0.03	DRAWN	KYUAN	3/14/21
			CHECKED		
			ENG APPR.		
			MFG APPR.		
		INTERPRET GEOMETRIC TOLERANCING PER:	Q.A.		
		MATERIAL Aluminum	COMMENTS: WATERJET		
NEXT ASSY	USED ON	FINISH Rough			
APPLICATION		DO NOT SCALE DRAWING			

TITLE:
Rig Joiner Plate

SIZE	DWG. NO.	REV
A	RIG_1004	B
SCALE: 1:1	WEIGHT: 0.16 lb	SHEET 1 OF 1